Upregulating Aggregation-Induced-Emission Nanoparticles with Blood–Tumor-Barrier Permeability for Precise Photothermal Eradication of Brain Tumors and Induction of Local Immune Responses

Zhang, Ming; Wang, Wentao; Mohammadniaei, Mohsen; Zheng, Tao; Zhang, Qicheng; Ashley, Jon; Liu, Shunjie; Sun, Yi; Tang, Ben Zhong

Published in:
Advanced Materials

Link to article, DOI:
10.1002/adma.202008802

Publication date:
2021

Document Version
Peer reviewed version

Upregulating Aggregation-Induced Emission Nanoparticles with Blood-Tumor-Barrier Permeability for Precise Photothermal Eradication of Brain Tumors and Induction of Local Immune Responses

Ming Zhang, Wentao Wang, Mohsen Mohammadniaei, Tao Zheng, Qicheng Zhang, Jon Ashley, Shunjie Liu*, Yi Sun*, Ben Zhong Tang**

Dr. M. Zhang, Dr. W. T. Wang, Dr. M. Mohammadniaei, Dr. T. Zheng, Dr. J. Ashley, Prof. Y. Sun
Department of Health Technology, Technical University of Denmark, Kongens Lyngby, DK-2800, Denmark
E-mail: wentwa@dtu.dk; suyi@dtu.dk

Prof. S. J. Liu
Key Laboratory of Polymer Ecomaterials, Changchun Institute of Applied Chemistry, Chinese Academy of Sciences, Changchun 130022, China; University of Science and Technology of China, Hefei 230026, China;
E-mail: sjliu@ciac.ac.cn

Q. S. Zhang
Jiangsu Collaborative Innovation Center for Biomedical Functional Materials, School of Chemistry and Materials Science, Nanjing Normal University, Nanjing 210023, P. R. China

Prof. B. Z. Tang
Hong Kong Branch of Chinese National Engineering Research Center for Tissue Restoration and Reconstruction, Department of Chemistry, The Hong Kong University of Science and Technology, Clear Water Bay, Kowloon, Hong Kong, 999077 China
E-mail: tangbenz@ust.hk

Keywords: photothermal therapy, glioblastoma, magnetic resonance, immune response

Compared to the other tumors, glioblastoma (GBM) is extremely difficult to treat. Recently, photothermal therapy (PTT) has demonstrated advanced therapeutic efficacies. However, due to the relatively low tissue penetration efficiency of the laser light, its applications in deep-seated tumors are still challenging. Herein, aggregation-induced emission nanoparticles (BK@AIE NPs) are synthesized, featuring selective penetration to the blood-tumor-barrier (BTB) and strong absorbance in the near-infrared region (NIR). The Bradykinin (BK) ligand can prompt BTB adenosine receptor activation, which enhances transportation and accumulation inside tumors, as confirmed by T1-weighted magnetic resonance (MR) and fluorescence imaging. The BK@AIE NPs exhibit high photothermal conversion efficiency

upon irradiation at 980 nm with NIR laser, enabling treatment of deep-seated tumors. The tumor progression can be effectively inhibited to extend the survival spans of mice after the spatiotemporal PTT. The NIR irradiation can eradicate the tumor tissues and release tumor-associated antigens. It is observed that PTT treatment of micebearing GBM activates natural killer (NK) cells, CD3+ T cells, CD8+ T cells, and M1 macrophages in the GBMs area to elevate the therapeutic efficacy. This study demonstrates that NIR-assisted BK@AIE NP is a promising strategy for the improved systematic elimination of GBMs and activation of local brain immune privilege.

1. Introduction

Owing to the presence of the blood tumor barrier (BTB) and the lack of efficient treatment strategies, glioblastoma (GBM) is currently one of the most devastating cancers.[1-3] The challenges of GBM treatment include (i) the high infiltration and aggressive nature of GBM, which results in the unsatisfactory remission by using traditional treatment methodologies (surgery, adjuvant chemo, or radiotherapy); (ii) the barrier of BTB, which makes it difficult for the delivery of diagnostic and therapeutic agents.[4, 5] Numerous efforts have been devoted to facilitate drugs to cross the BTB. Receptor-mediated transcytosis that utilizes the receptors/transporters expressed on BTB, is a popular approach.[6, 7] However, many of these receptors are commonly expressed in several tissues and cell types, resulting in harmful uptake of peripheral organ. In addition, due to the limited number of cellular membrane transporters and the complicated intracellular transport process, the intracellular transport capacity is rather low. Most methods are invasive and cause a non-specific increase in permeability throughout the central nervous system (CNS).[8] An alternative strategy is to modulate the permeability of BTB, which potentially allows the delivery of larger amount of therapeutics. In that regard, we found that kinin B1 receptor (B1R) is of particular interest. Kinin peptides are natural modulators of the tone and permeability of vessels.[9] The biological

tasks of kinins are mediated through the activation of G-protein coupled receptors (GPCR) called the B1R and B2R. B2R exhibits constitutive expression in numerous tissues. On the contrary, except for CNS, B1R is almost undetectable under physiological conditions.[10] Moreover, B1R is proven to be inducible and expressed in major inflammatory diseases, including cardiovascular disease and cancer. Therefore, B1R is likely to serve as a pharmaceutical target to minimize collateral effects.[11] Some researchers have developed B1R-targeted smart drug delivery NPs for cancer and other B1R related cancer diseases treatments.[12, 13] It is noteworthy that GBM is in a zone of inflammation that maintains tumor proliferation and angiogenesis, while the process partly relies on GBM-derived cytokines, which may trigger B1R activity on the microcirculatory system of brain tumors. As a result, GBM cells as well as the surrounding brain capillary endothelial cells show an over expression of B1R.[14] Therefore, we envisioned that the kinin ligand could bind to the B1R on the blood vessel in GBM areas, thus locally increasing the permeability of the BTB. In addition, the kinin ligand can also specifically target the GBM cells. Conjugating the B1R kinin ligand with therapeutics or nanoparticle (NP)-based drug delivery systems therefore would present a completely new way to safely and effectively deliver drugs to tumors in CNS.[15, 16]

NP-based photothermal therapy (PTT) has been demonstrated with a high degree of efficiency to selectively ablate the tumors.[17] Recently, several strategies of PTT have been proposed for brain tumors. As the most widely used clinical thermal ablation method, PTT is also utilized for treating recurrent or deep brain tumors.[18, 19] Whereas in these studies, the general power density of 808 nm laser was above 1.5 W/cm^2, which was far beyond the safe 0.33 W/cm^2 value.[20] This is because the dense skull and scalp can cause severe attenuation of the incident light, such that only lasers with high power density can reach the therapeutic threshold to penetrate these tumor tissues. One option to improve the light penetration in PTT, is to change the wavelength of a laser from 808 nm to 980 nm, as the living tissues would be more

transparent for the 980 nm laser.[21-23] However, an unresolved issue to apply 980 nm laser in brain-tumor PTT treatment is the lack of secondary NIR (NIR-II) photothermal therapeutic agents.[24, 25]

Fortunately, aggregation-induced emission (AIE)-active luminogens (AIEgens), as a new kind of fluorophore with freely motioned molecular vibrators or rotators in structure, would be an ideal option as a NIR-II photothermal therapeutic agent. The AIEgens has a potential tunable performance by promoting or inhibiting the intramolecular motions, and NIR-II absorbing AIEgens have been demonstrated.[26-30] Furthermore, organic theranostic agents can be fabricated into NPs forms to obtain ideal preferential accumulation and blood circulation time in the tumor regions.[31, 32] Although synthesis of AIEgen NPs may partially restrict the intramolecular motion of AIEgens, AIE NPs can form in loose packing configurations to keep intramolecular motions active based on their inherent twisted propeller-like conformations.[33-35] This, in turn, makes AIEgens suitable for balancing energy dissipation and multifunctional phototheranostics.[36-38] Thus we hypothesized that AIE NPs could function as effective NIR-II PTT agents. In addition, according to recent preliminary clinical trial studies, PTT can generate a tumoricidal immunological effect by releasing tumor-associated agents from the residue after hyperthermia of tumor cells.[39-41] Inspired by such interesting findings, we also postulated that the tumor-associated antigens generated *in situ* after NIR-II PTT treatment would activate the immune response in the GBM region.

Herein, the [des-Arg^9]Bradykinin (BK, a type of B1R agonist) decorated photostable and biocompatible conjugated AIE NPs which has strong absorption in the NIR-II window were designed for brain tumor treatment using a synergetic strategy of PTT and local immune response activation (**Figure 1A**). A higher penetration efficiency into the scalp and skull for 980 nm laser was observed as compared with the common 808 nm laser, which is in agreement with previous literatures.[42, 43] In addition, owing to the active targeting effect of the BK ligand, a real-time multi-modal imaging system assisted clear pinpointing of the

aggregation of BK@AIE NPs in the GBM. After spatiotemporal PTT, the tumor progression was effectively inhibited and the immune response was significantly activated. Finally, BK@AIE NPs-mediated PTT further stimulated the activation of T lymphocytes, natural killer (NK) cells, and enhanced M0 macrophages differentiating into M1 macrophages (MΦ) (Figure 1B). To the best of our knowledge, this is the first report of using AIE NPs with covalently bonded B1R agonists to treat brain tumors and activate the local immune response.

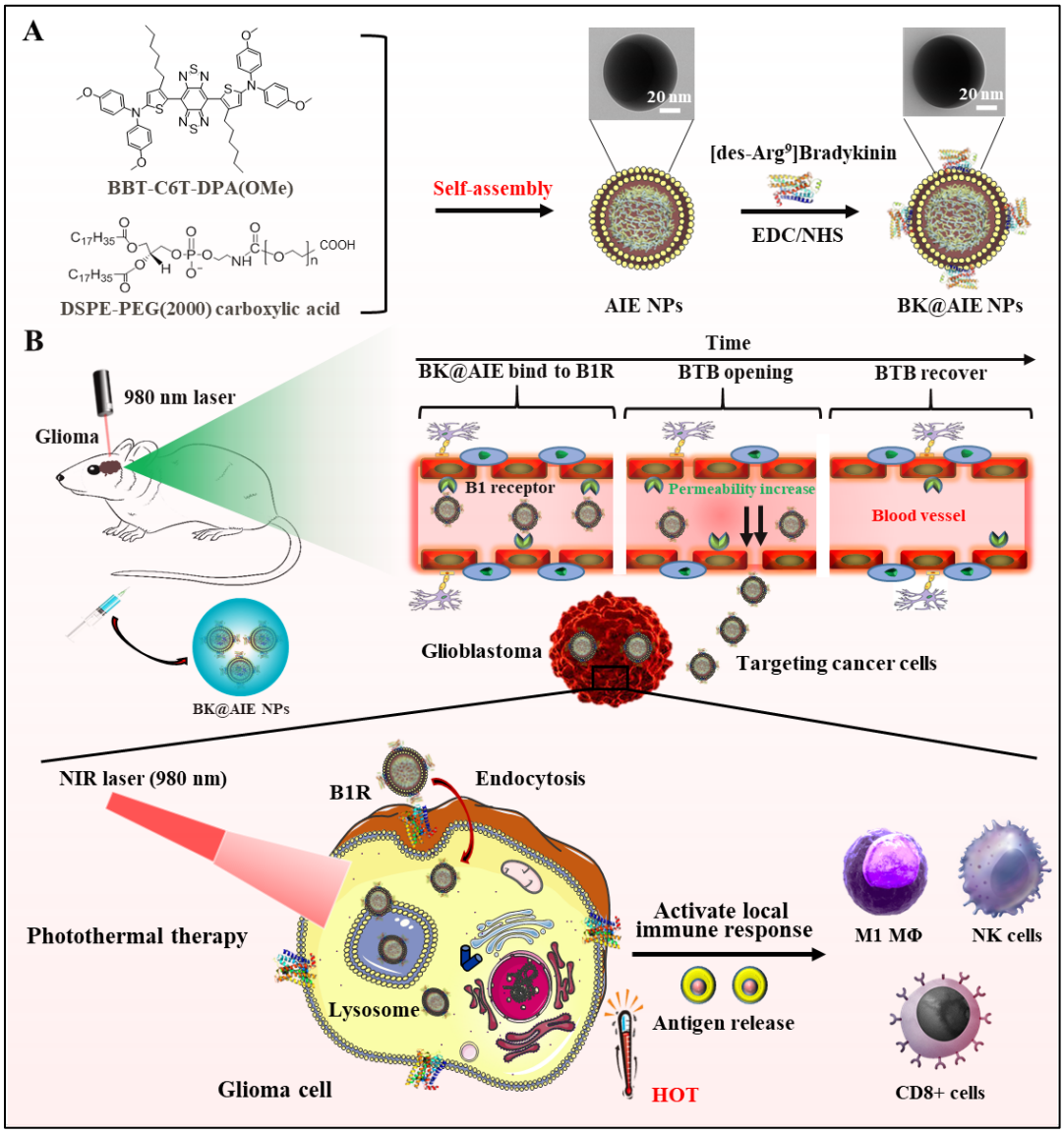

Figure 1. Schematic diagram of (A) fabrication procedure of BK@AIE NPs, and (B) synergetic treatment of brain tumors using PTT and local immune response activation.

2. Results and discussion

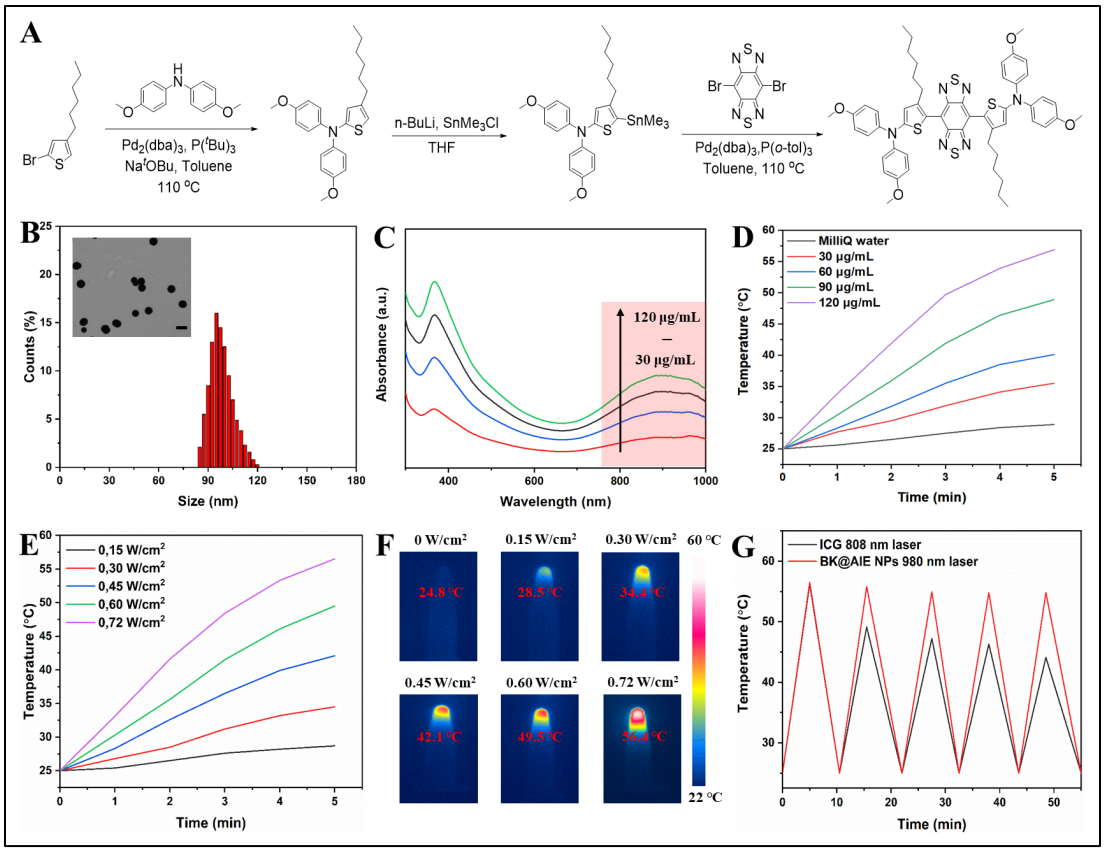

Figure 2. (A) Synthetic procedure of BBT-C6T-DPA(OMe). (B) DLS data of BK@AIE NPs. Inset shows the TEM image of BK@AIE NPs. Scale bar: 100 nm (C) UV-Vis spectra of BK@AIE NPs at different concentrations. (D) Photothermal properties of BK@AIE NPs at various concentrations under 980 nm laser (0.72 W/cm^2). (E) Photothermal effects of BK@AIE NPs (120 μg/mL) at different laser powers. (F) Infrared thermal images of BK@AIE NPs at different laser powers for 5 min. (G) Temperature variation of free ICG and BK@AIE NPs over five cycles of repeated laser irradiation (switch on/off).

The synthetic routes of BBT-C6T-DPA(OMe) are given in **Figure 2A**. Its structures and characterization results are shown in Figure S1-3. Compared with the intramolecular rotation, the intramolecular bond stretching vibration in BBT-C6T-DPA(OMe) small molecules is less sensitive to the external environmental constraints, which leads to its great advantageous in improving the heat generation inside the NPs. To investigate more about the photothermal characteristics at the morphological level, we synthesized the AIE NPs through a nanoprecipitation method using amphiphilic copolymers (DSPE-PEG2000), a type of biocompatible copolymers that have been used frequently in the drug delivery field, as the doping matrix (Figure 2B). In addition, the matrix endued AIEgens with desirable blood

circulation time and excellent colloidal stability. To increase the permeability of the BTB and target to the GBM cells, BK was modified on the AIE NPs surface *via* EDC/NHS coupling. The BK modified surface would enhance the cell uptake for NPs then resulting in ameliorating therapy outcomes. The change in Zeta potential verified that BK was successfully loaded on the surface of the AIE NPs (Figure S4). Stability is important for the biomedical application of BK@AIE NPs. The BK@AIE NPs have no flocculent precipitation in various physiological solutions (Figure S5A). Meanwhile, BK@AIE NPs, dissolved in various physiological solutions, displayed no changes in average size (Figure S5B) and zeta potential (Figure S5C) after 14 days in storage, indicating great stability. TEM and dynamic light scattering (DLS) revealed that the BK@AIE NPs exhibited uniform spherical morphology with diameters of c.a. 100 nm (Figure 2B). Distinctly EDS mapping images of BK@AIE NPs were seen (Figure S5D). Within individual BK@AIE NPs, S, N, and P elements were homogeneously distributed, which indicated that the AIEgens were successfully assembled.

We assessed three characteristics of BK@AIE NPs to evaluate their feasibility for PTT: (i) absorption properties in the NIR region, (ii) photostability, and (iii) photothermal conversion (PC) efficiency. From the UV-Vis spectra of BK@AIE NPs in Figure 2C, two distinct peaks can be seen in the UV and NIR regions. Interestingly, a broad absorption was observed within the NIR region with the maximum value at c.a. 980 nm, making it very applicable for NIR-II PTT. Evidently, the change in NP concentration from 30 to 120 μg/mL increased the measured absorption intensity. In this work, we selected a commercially-available and compatible 980 nm continuous laser to study the NIR-II photothermal effect of BK@AIE NPs with different concentrations under different laser powers. In Figure 2D-F, the temperature of BK@AIE NPs solutions increased dramatically with 980 nm laser irradiation and with an increase in BK@AIE NP concentration. The temperature of BK@AIE NPs solutions (120 μg/mL) increased by 31.3 ℃ with 5 min irradiation, while the temperature in the water group

increased by 3.2 ℃ (Figure 2D). Figure 2E, F illustrates the recorded temperature of BK@AIE NPs suspension as a function of laser power. A rapid increase in BK@AIE NPs temperature within 5 min was observed, from which, 0.72 W/cm^2 laser power represented an appropriate localized temperature of 56.4 ± 2.1 ºC for further analysis. Moreover, the photothermal stability of BK@AIE NPs was evaluated. As shown in Figure 2G, the PC properties of BK@AIE NPs showed no significant change after five cycles of NIR irradiation, whereas for the free indocyanine green (ICG) a gradual decrease of temperature over the five cycles was seen, suggesting good photothermal stability of our developed BK@AIE NPs.

To verify the superiority of the 980 nm laser over the 808 nm laser for PTT, their penetration ability was evaluated via irradiating various tissues. As shown in Figure S6, 7, the 980 nm laser represented significantly deeper penetration than that of the 808 nm laser under the same tissue thickness. For instance, within 3 mm chicken tissue, about 41% of the 980 nm laser energy was successfully kept, while this was only around 28% for the 808 nm laser (Figure S6). Figure S7 indicates the results of the laser penetration rate through the mice' skulls and scalps. In the mice skull group, tissues treated with 980 nm laser (85%) retained more light energy than the 808 nm laser (78%) treated group. Similarly, through mice skulls together with the scalps, tissues treated with 980 nm laser (48%) lost less light energy than the 808 nm laser (31%) treated group. Therefore, these data suggest that 980 nm PTT should be more effective in treating brain tumors.

It is well known that active targeting could efficiently improve the targeted ability for nanoscale formulations during the drug delivery process. B1R, inducible prototypical GPCR regulates the permeability of vessels in brain tumors.[44,45] Therefore, B1R was investigated as the specific biomarker on the AIE NPs for inflammatory tumor cells (**Figure 3A**). Here, we detected the expression of B1R in the U87-MG cell line and normal human astrocytes. Based on the immunofluorescence analysis, there is a significantly higher signal from B1R protein in U87-MG cells compared to the normal human astrocytes (Figure 3B). To verify the *in vitro*

BK@AIE NPs targeting efficiency, cyanine-5.5 (cy5.5) was chosen to modify the BK@AIE NPs for monitoring uptake *via* EDC/NHS coupling. The uptake of BK@AIE NPs was observed by a fluorescence microscope followed by quantitative data analysis using Image J software (Figure 3C). The results show a substantially higher cellular uptake of the BK@AIE NPs in U87-MG cells. These results show that the BK@AIE NPs specifically recognized U87-MG cells due to the interaction between BK and B1R. Similarly, the BK-based NPs could efficiently target U87-MG tumors *in vivo* rather than normal human astrocytes from the previous work.[46]

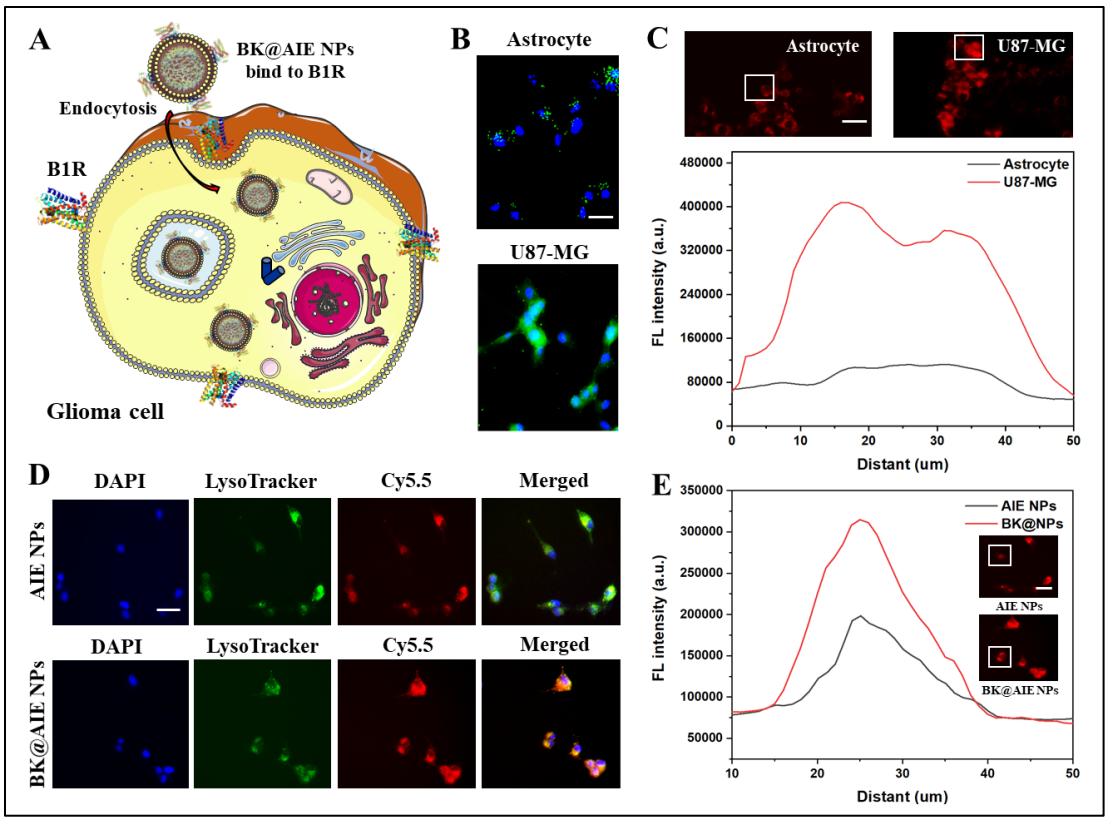

Figure. 3 (A) The proposed mechanism of BK@AIE NPs cellular uptake pathway. (B) Detection of B1R in U87-MG cells and normal human astrocytes. Scale bar: 20 μm (C) Laser scanning confocal microscopy (LSCM) images and quantitative fluorescence intensity of the *in vitro* cellular uptake of BK@AIE NPs cells in U87-MG cells and normal human astrocytes. Scale bar: 50 μm (D) LSCM images of U87-MG cells after incubation with AIE NPs and BK@AIE NPs for 4 h. Scale bar: 20 μm (E) The quantitative fluorescence intensity of U87-MG cells after incubation with AIE NPs and BK@AIE NPs by Image J. All NPs were labeled with cy5.5. Scale bar: 25 μm

The intracellular delivery NPs into the target site are critical factors for influencing their potential applications in biomedicine.[47, 48] Therefore, to further monitor the location of

BK@AIE NPs in the cancer cells, we conducted the co-localization analysis using U87-MG cells incubated with LysoTracker biomarkers and 4',6-diamidino-2-phenylindol (DAPI). BK@AIE NPs were labeled with cy5.5 in Figure 3D, and the endo/lysosomes were stained with LysoTracker Green dyes. The most pristine AIE NPs remained inside the lysosomes after incubating with the cells for 4 h, as displayed by the yellow dots in the merged LSCM images (overlap of red and green dots). In contrast, co-localization was reduced when analyzing the BK@AIE NPs, suggesting that BK@AIE NPs accumulated mainly in the lysosomes of U87-MG cells (Figure 3D). The cellular internalization efficiency of BK@AIE NPs was also evaluated by LSCM and the fluorescence signal was analyzed by Image J. In Figure 3E, the cellular uptake efficiency of BK@AIE NPs intensely relies on the B1R mediated endocytosis pathway. The red fluorescence intensity emitted by cy5.5 was stronger in the BK@AIE NPs group, indicating BK@AIE NPs has a higher cellular uptake in U87-MG cells. Meanwhile, the fluorescence signal was weaker after treating with AIE NPs. The above results suggested that the BK@AIE NPs group not only accelerated the NPs escaping from the lysosome but also improved the internalization efficiency.

Being similar to many other indexes, the dysfunction of mitochondria has been identified as a functional marker of cell apoptosis. Therefore, the dysfunction of mitochondria in U87-MG cells caused by BK@AIE NPs under 980 nm laser irradiation was examined before further evaluation of the *in vitro* photothermal therapeutic efficacy. The mitochondrial membrane potential (MMP) was introduced to monitor the degree of damage through staining with JC-1 (**Figure 4A**). Acknowledgment of the decreasing MMP always replies to the gathering of JC-1 monomer (green fluorescence) while the aggregation of JC-1 (red fluorescence) responds to a high MMP, which indicates a standard state. Moreover, the fluorescent shift of JC-1 from orange to green represents the occurrence of early apoptosis. As shown in Figure 4A, the approximate JC-1 aggregation through red fluorescence from different treatment groups suggested a negligible change of MMP in cells, as well as insignificant harm to the

mitochondria. However, the sharp increase in green fluorescence in the BK@AIE NPs plus 980 nm laser group, suggesting that the mitochondria were destroyed. Hence, we comprehended that the local hyperthermia from BK@AIE NPs plus 980 nm laser treatment accounted for the dysfunction of mitochondria, which means this system could inspire an efficient antitumor process by the targeted PTT outcome and enhanced cell apoptosis. Recently, the immunogenic cell death (ICD) sprang up to describe the state of immunogenic apoptosis and the active immune response. One of the characteristics of ICD is the increased surface exposure of calreticulin proteins (CRT) following the extensive degree of damage. As a result, CRT exposure servers as a phagocytic calling signal to provoke an internal immune response.[49, 50] Based on this knowledge, we further investigated the PTT therapeutic effect from BK@AIE NPs plus NIR-II laser in GBM cells. Immunofluorescence assays (Figure 4B) showed that the higher level of CRT only occurred in the BK@AIE NPs plus laser radiation group, indicating their excellent photothermal effect. These results demonstrate that BK@AIE NPs based PTT can induce apoptosis among U87-MG cells while enhancing the release of damage-associated molecular patterns. Afterward, the *in vitro* antitumor efficiency of BK@AIE NPs was also confirmed by MTT assay, calcein-AM/PI staining, and tumorsphere formation. It was found that BK@AIE NPs treated cells showed remarkably reduced viabilities by increasing the BK@AIE NP concentration and laser power intensities (Figure 4C). However, incubation of U87-MG cells for 24 h without laser irradiation caused a minimal impact on the cell viability test. To investigate PTT *in vitro*, green-emissive calcein-AM and red-emissive propidium iodide (PI) staining was applied to distinguish live and dead cells, respectively (Figure 4D). Upon light irradiation at 980 nm for 5 min, the green fluorescence decreased upon increasing the BK@AIE NPs concentration and laser power intensities. In Figure 4D, almost all the cells were apoptotic/dead after treatment with 120 μg/mL BK@AIE NPs under 980 nm laser irradiation (5 min, 0.72 W/cm^2). Next, we examined tumorsphere formation of GBM cells by incubating with different concentrations of

BK@AIE NPs after 980 nm laser irradiation (5 min, 0.72 W/cm^2). Treatment of U87-MG cells with BK@AIE NPs strongly inhibited their ability to form tumorspheres (Figure 4E). The above results indicated that the BK@AIE NPs group not only exerted their functions to kill cancer cells but also inhibited tumor recurrence.

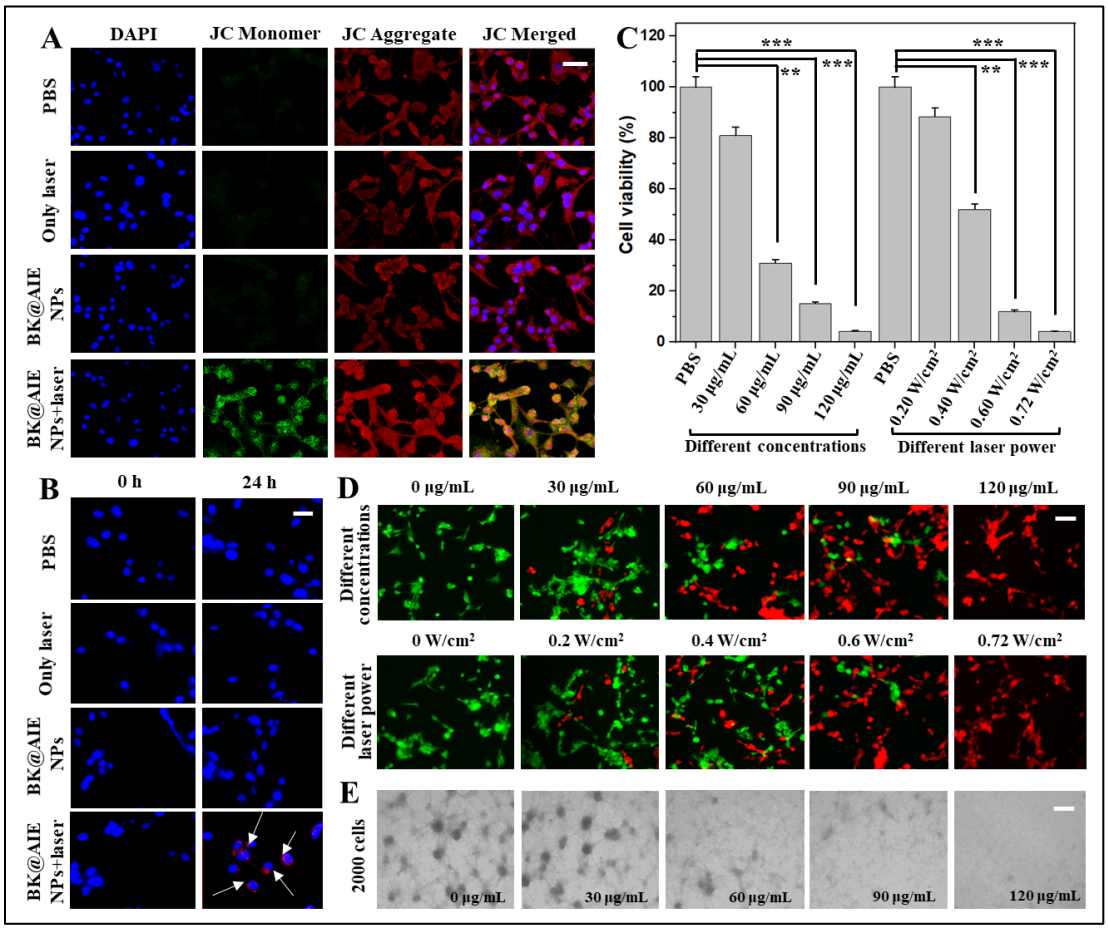

Figure 4. (A) Fluorescence images showing the MMP changes of U87-MG cells under different treatments. Scale bar: 50 μm (B) CRT expression of U87-MG cells after various treatments. Scale bar: 20 μm (C) Relative viabilities and (D) live/dead staining of U87-MG cells in different treatment groups. U87-MG cells were incubated with different concentrations of BK@AIE NPs, and then refreshed media and irradiated with the 980 nm laser (5 min, 0.72 W/cm^2). U87-MG cells were incubated with BK@AIE NPs (120 μg/mL), and then refreshed cell culture media and irradiated with the 980 nm laser at various laser power densities for 5 min. Afterward, cells were re-incubated for an additional 24 h before performing the MTT assay, ***p <0.001 and **p <0.01. Scale bar: 50 μm. (E) Images of formatted tumorspheres among U87-MG cells after different treatments. Scale bar: 500 μm

The penetration of BTB as one of the most challenging natural obstacles for drug delivery was also evaluated by constructing the U87-MG/human vascular endothelial cells (HUVECs) co-culture model. HUVECs were given angiogenesis characteristics when coexisting with U87-

MG cells (**Figure 5A**). The AIE NPs and BK@AIE NPs were added to the apical chamber of the simulated BTB. The agonist-mediated dynamic penetration of AIE NPs with and without BK were quantitatively evaluated by detecting the fluorescence intensity in the basal chamber after adding these NPs into the apical chamber at various time points during 24 h. It was shown that the crossing efficiency of BK@AIE NPs changing with the BTB permeability (Figure 5A). We monitored the BTB crossing efficiency of AIE NPs and BK@AIE NPs within 24 h of post-treatment. BK@AIE NPs showed higher crossing efficiency, which was 5.3 times higher than that of AIE NPs. The results suggested that BK@AIE NPs could improve their passing amounts by upregulating BTB permeability.

Moreover, the specific targeting towards U87-MG cells and tumoricidal effects induced by NIR-II laser of the BK@AIE NPs were evaluated in the presence of normal human astrocytes co-cultured in a basal chamber (Figure 5B). As the control experiment, we also plated U87-MG cells and normal human astrocytes incubated with the BK@AIE NPs. The exposure of BK@AIE NPs-treated U87-MG cells with laser irradiation resulted in around 98% of cell loss, which was significantly higher than that of normal human astrocytes (c.a. 49%). Interestingly, the amounts of normal human astrocyte cells stayed healthy in the mixed normal human astrocytes/U87-MG group. These results demonstrate that, with an effective cancer cell targeting molecules, PTT could serve as a precise strategy to cure GBM with minimal damage to the adjacent tissues.

Hemolysis rate as a standard parameter was evaluated to give support to the available hemocompatibility of BK@AIE NPs, which was one of the criteria for further bioapplication. To be a usable and safe therapeutic agent, the hemolysis rate should be kept below 5% to avoid the hemoglobin-release and thrombosis-formatting. As Figure S8A shows, the hemolysis rate region of BK@AIE NPs changed from 1.02% to 1.45% at different concentrations, resulting in no impacts on hemolysis. It should be noted that the morphological changes of nanomaterials after interaction with red blood cells (RBCs) are

another vital factor to evaluate their hemocompatibility. Fragmentation or aggregation of RBCs indicates the incompatibility of nanomaterials. Here, we gave samples for the normal and damaged morphologies of RBCs (Figure S8B). RBCs incubated with PBS was set as negative control while incubated with water was the positive control. Similar to the negative control, RBCs in BK@AIE NPs incubation groups kept the normal circular morphology rather than any morphological destruction. In addition, U87-MG, normal human astrocytes, and HeLa cells were incubated with BK@AIE NPs in a series of concentrations (Figure S9A). BK@AIE NPs showed their bio-safety among these cell lines, even at a concentration as high as 120 μg/mL. The morphology of the U87-MG, normal human astrocytes, and HeLa cells was in a normal state when the concentration of BK@AIE NPs reached 120 μg/mL (Figure S9B). Above all, we demonstrated that BK@AIE NPs possess excellent biocompatibility.

To completely advance the therapy of PTT to malignant GBM, we need to overcome the restriction from BTB to promote the delivery process. B1R is spontaneously introduced to our system as it is reported to regulate the microstructure of brain tumors by changing the permeability of vessels. By analyzing with Western blot, we found that B1R protein exhibited a higher level in U87-MG tumor tissues than in normal tissues (Figure S10). Normal brain tissues showed negligible levels of B1R. Therefore, we studied the capability of BK@AIE NPs to temporarily modulate BTB permeability *in vivo* by monitoring ethidium bromide (EB) penetration. EB extravasation represents serum albumin extravasation from blood vessels as they stably interplay with each other.[51] Mice were intravenously injected with AIE NPs or BK@AIE NPs, following by subsequent injection of EB. After 6 h, the mice brains were separated and used for performing histologic analysis. We found that the BK@AIE NPs treatment significantly enhanced the BTB permeability, resulting in EB vascular penetration and a more homogeneous distribution of EB within the tumor interstitium (Figure 5C). We also noted that AIE NPs and PBS treatment could not enhance EB vascular penetration and improve their distribution profile. These results suggested that the BTB permeability could

only be improved under the treatment of BK@AIE NPs. It might be associated with the binding of B1R agonists ([des-Arg^9]Bradykinin) to their receptors in brain tumor areas. This interaction results in increased permeability of BTB by inspiring a set of secondary reactions and expression of related proteins in the transcellular or paracellular pathway.

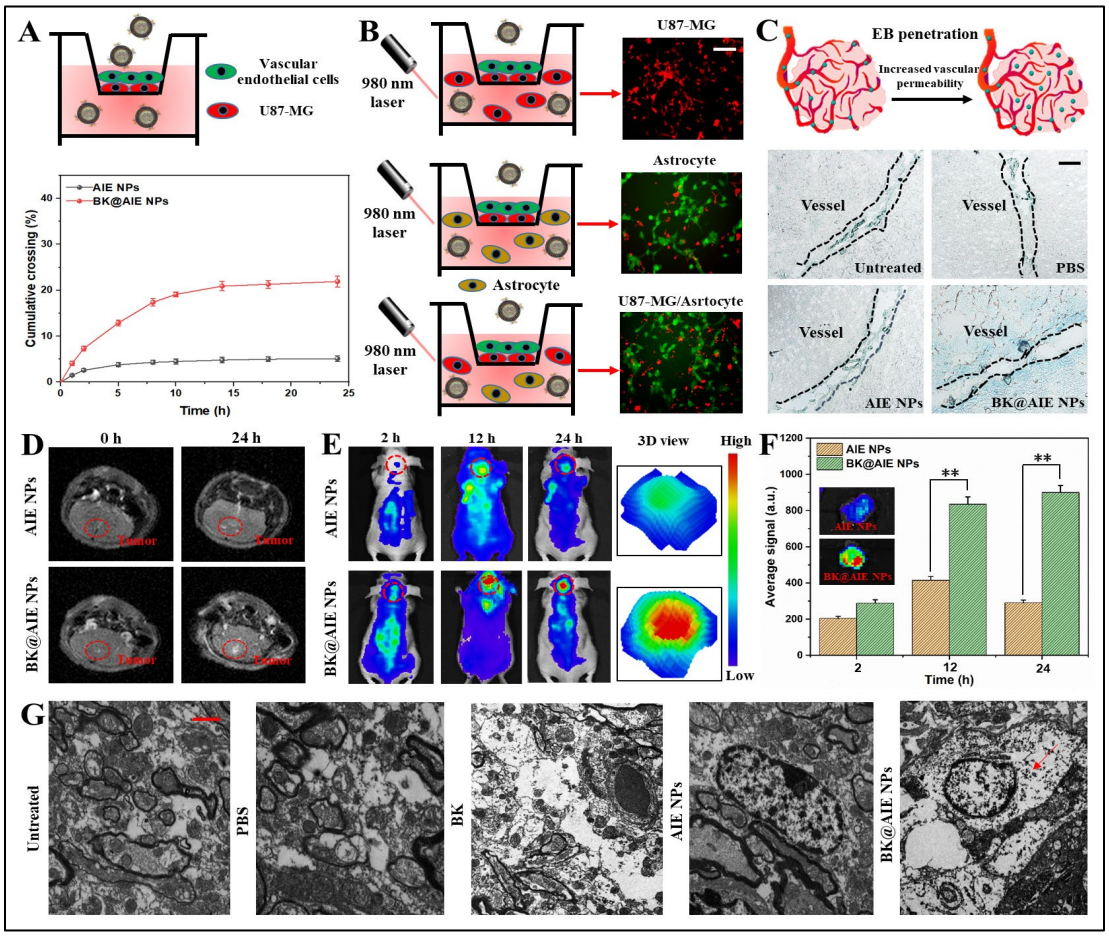

Figure 5. (A) Schematic of the transwell assay to evaluate co-cultured cell permeability. Evaluating BTB crossing dynamics of AIE NPs and BK@AIE NPs (0–24 h). (B) U87-MG cells specifically targeted by the BK@AIE NPs and the normal human astrocytes were mixed and co-cultured in the basal chamber. The viabilities of U87-MG, normal human astrocytes/U87-MG, and normal human astrocytes are shown after the PTT. Scale bar: 100 μm (C) EB staining of brain sections after different treatments. Scale bar: 50 μm (D) MR images for the mouse brain in different groups. (E) *In vivo* fluorescence imaging from mice at different time points after AIE NPs and BK@AIE NPs injections, respectively. (F) Quantitative fluorescence analysis in the tumor site at different time points after treating with AIE NPs and BK@AIE NPs. Inset is the fluorescence imaging of the brain after AIE NPs and BK@AIE NPs injections for 24 h, **p <0.01. (G) Bio-TEM images of the brain blood vessels after AIE NPs and BK@AIE NPs injections for 8 h. The red arrows represent BK@AIE NPs. Scale bar: 5 μm

In our current and various previous studies, we identified that gadolinium ion (Gd^{3+}) anchored on NPs produced by the ion complexation can provide strong contrast for MR imaging.[52, 53] As expected, *in vitro* studies showed a brightening effect in a concentration-dependent manner after treating with BK@AIE NPs samples, which gave support for their potential use in T1-weighted MR imaging (Figure S11). After intravenous injection of AIE NPs and BK@AIE NPs into U87-MG tumor-bearing mice, a dramatically bright appearance was detected in the tumor region with *in vivo* MR imaging, which attributed to the high tumor accumulation of NPs after systematic administration (Figure 5D). It was observed that the MR signal was about twofold higher in the BK@AIE NPs group, which gave clear evidence that BK played the key role in crossing BTB *in vivo*. The MR signal in the AIE NPs group benefits from the EPR effect, as compared to that of the BK@AIE NP group. The quantitative analysis of the region of interest (ROI) is shown in the MR imaging way (Figure S12).

Next, we evaluated the active crossing ability of BK@AIE NPs *in vivo* by intravenous injection with an orthotopic U87-MG tumor-bearing mice model. In Figure 5E, the higher fluorescence signal in the BK@AIE NP group suggested the excellent targeting ability of BK. Meanwhile, it also proved that the conjugation of BK made up for the limited penetration from the BTB to the passive accumulation of AIE NPs from the EPR effect. The quantitative analysis for the brain accumulation of BK@AIE NPs and AIE NPs is shown in Figure 5F. Remarkably, the average signal in tumors achieved an almost threefold higher effect in the BK@AIE NPs treatment group after 24 h. These results validated that BK@AIE NPs have prominently enhanced BTB penetration and tumor accumulation. Furthermore, we studied the *in vivo* behavior of BK@AIE NPs using animals. Prolonged circulation of NPs in the bloodstream is essential to improve the probability of entering the tumor and accumulation therein. We intravenously injected BK@AIE NPs into the U87-MG glioma-bearing mice. To further verify that nanoparticles increase the permeability of blood vessels and cross the BTB, biological TEM was used to observe the internal structure of blood vessels in the brain.

Compared with the AIE NP group, we observed that the vascular tissues in BK and BK@AIE NP groups were relatively loose. As expected, the BK@AIE NPs are concentrated in the intercellular space (Figure 5G). Besides, the behavior of BK@AIE NPs in blood was detected at different time points during 24 h after the injection. It seemed that they were still at a reasonably high level after 24 h, even in spite of the general gradually downward trend (Figure S13).

We next evaluated the feasibility of PTT using BK@AIE NPs in conventional xenograft tumor mice. U87-MG cells were inoculated into the right oxter of male BALB/c nude mice as a conventional xenograft tumor model. The infrared thermal camera was applied to record the local temperature in tumor sites to supply evidence of the substantially higher ability of PTT from AIE NPs. Meanwhile, the conjugated BK endowed more AIE NPs to gather the tumor site, which assumed a hyperthermal effect with a local tumor temperature of 52.8 °C under NIR-II exposure for 5 min while the AIE NPs group was around 49 °C (**Figure 6A**, S14). These observations demonstrated that our BK@AIE NPs could successfully target brain tumor cells. To further evaluate the PTT efficiency, BK@AIE NPs, AIE NPs, and PBS were intravenously injected at predetermined times, respectively. After 24 h, 980 nm laser (0.72 W/cm^2) was used to irradiate the tumor sites for 5 min to assess the impacts from the laser irradiation to tumor propagation. As a result, only irradiation of NIR-II laser did not cause tumor suppression (Figure S15). Moreover, tumor volumes were recorded under different treatments showing that the growth of tumors could be inhibited by the individual PTT effect from the NIR-II laser (Figure 6B). However, a more remarkable decrease occurred in the BK@AIE NPs plus NIR-II laser group, this result was also reflected in the tumor volumes measurement during 18 days (Figure 6B, S15A).

The responding histological analysis of tumor tissues in every treatment group was performed to deeply understand the therapeutic effect. As shown in Figure S15B, H&E stained tumor sections showed obvious cytoplasmic leakage and nuclear atrophy of apoptotic cells from the

BK@AIE NPs and PTT treated group. As an available therapeutic agent, the bio-safety of BK@AIE NPs also needed to be assessed. Body weights, identified as an assessment index, were recorded in all the groups during the therapeutic process, which represented the extent of side effects on mice (Figure S16). As recorded, mice in different groups slightly increased after 18 days, referring to a healthy life cycle. In Figure S17, H&E staining analysis for the major organs agreed with the above results, as no group showed necrosis or morphology changes. This result also could be confirmed by the routine blood examination (Figure S18), in which all the groups kept normal physiological activity. As a conclusion, we demonstrated that the fabricated BK@AIE NPs exerted no obvious *in vivo* toxicity.

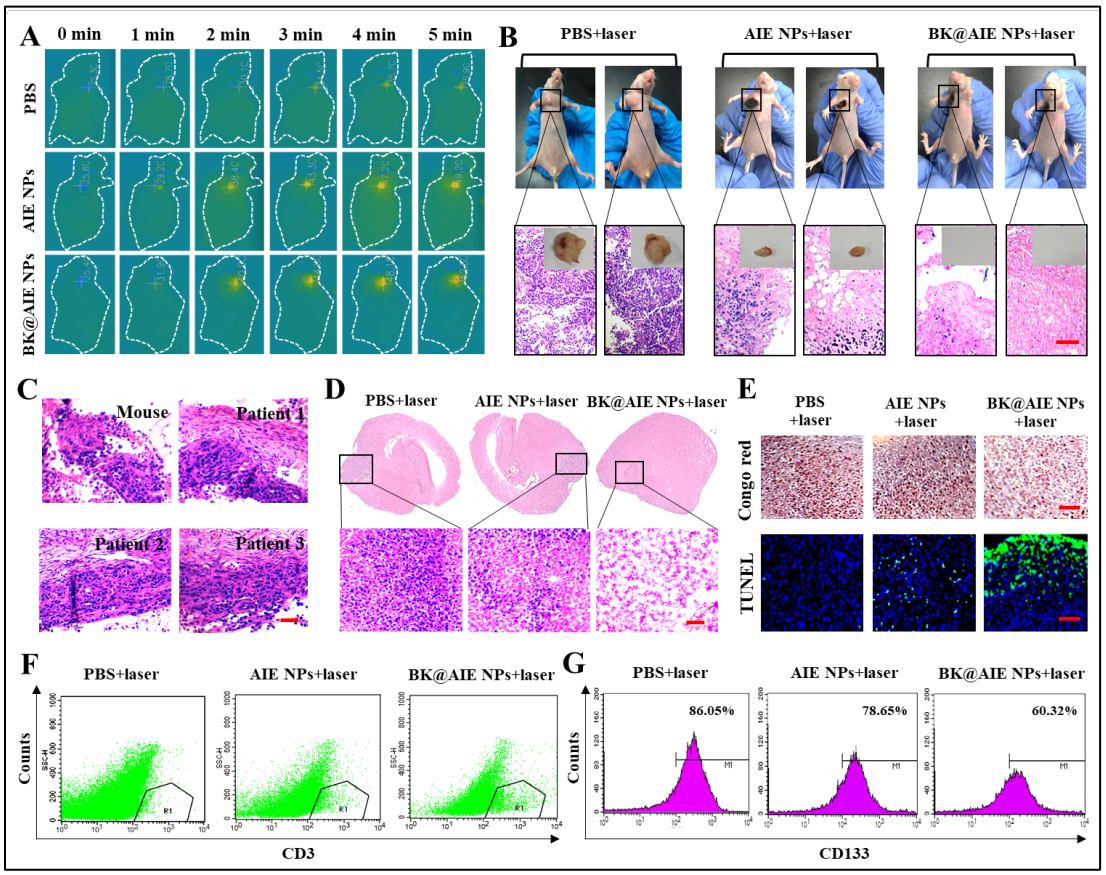

Figure 6. (A) Infrared thermographic maps of tumors in the mice were measured 5 min after continuous laser irradiation (980 nm, 0.72 W/cm^2). (B) Representative photos of U87-MG gliomabearing mice treated with PBS, AIE NPs, and BK@AIE NPs following by NIR-II laser irradiations. Scale bar: 100 μm (C) Histological observations of brains of orthotopic GL261 glioma-bearing mice and GBM patients. Scale bar: 100 μm (D) Histological observations of brains of orthotopic GL261 glioma-bearing mice treated with PBS plus laser, AIE NPs plus laser, and BK@AIE NPs plus laser. Scale bar: 100 μm (E) Congo red and TUNEL staining of brains of orthotopic GL261 glioma-bearing mice treated with PBS plus laser, AIE NPs plus

laser, and BK@AIE NPs plus laser. Scale bar: 100 μm (F) Quantification of the intratumoral proliferation of CD3+ T cells by flow cytometric. (G) Histograms illustrating the percentage of annexin V expression in CD133+ cancer stem cells (CSCs).

In addition, the *in vivo* therapeutic effect of BK@AIE NPs was evaluated in orthotopic brain tumor models, which were constructed by inoculating glioma 261 (GL261) cells into the striatum of female C57BL/6J mice. The successful establishment of tumor models was verified by comparing the pathological sections of patients and mice (Figure 6C). The patient's tumor tissue was similar to that of mice. We also tested the expression level of B1R in the tumor tissues (Figure S19). The B1R expression level was significantly higher in GL261 tumor tissue samples compared to normal tissue samples. Normal brain tissues showed negligible levels of B1R. Mice bearing orthotopic glioblastomas were treated with various solutions and then exposed to laser irradiation (980 nm, 0.72 W/cm^2) for 5 min. By recording the temperature of the tumor sites, we observed increased temperature of more than 15 °C only in the BK@AIE NPs plus laser treatment group (Figure S20). AIE NPs plus laser and PBS plus laser groups were used as control (n = 10 per group). The high therapeutic effect of BK@AIE NPs plus laser group was also confirmed by histological staining, exhibiting the most apoptosis of tumor cells and a reduction in proliferation (Figure 6C, D). Moreover, the strong tumoricidal ability of BK@AIE NPs plus laser treatment was also identified in the H&E and Congo red staining results, in which nearly the whole tumor tissue disappeared, consistent with the tumor margin analysis of TUNEL staining (Figure 6E). The obviously strong green fluorescence signal presented due to the increase in apoptotic cells in tumor tissue, while cells around the normal tissue stayed normal, verifying the minimal damage of PTT to the healthy cells. The survival time of GBM bearing mice under different treatments was also measured to evaluate the anti-glioma efficacy in Figure S21. The medium survival time of BK@AIE NPs plus laser was 48 days, suggesting that BK@AIE NPs plus laser significantly extended animal survival time in comparison with PBS plus laser (25 days)

and AIE NPs plus laser (30 days). These results indicated that BK conjugated AIE NPs demonstrated a desirable therapeutic effect here that could serve as a promising drug delivery system for glioma treatment.

Accordingly, PTT-induced dead cancer cells release tumor-derived antigens could stimulate the host immune system, lead to acute inflammation and leukocyte infiltration to tumors, inspire T cells, M1 MΦ, and NK cells.[54, 55] Oxaliplatin was generally used to induce ICD in mouse colorectal cancer models.[56, 57] The brain tumors near the endpoint of mice after PTT were harvested to further investigate the local immune response. CD3+ T cells, CD8+ T cells, CD4+ T cells, M1 MΦ, and NK cells were revealed by flow cytometry. The percentage of infiltrating CD3+ T cells (Figure 6F), CD4+ T cells, and CD8+ T cells (Figure S22) concerning the whole cells in the tumors sharply increased in mice with BK@AIE NPs plus laser treatment. Interestingly, AIE NPs plus laser increased tumor-infiltrating CD3+ and T CD8+ T cells in tumors rather than CD4+ T cells. Activation of brain immunity contributed to a significant growth in tumor M1 MΦ and NK cells. Particularly, M1 MΦ-generated iNOS is responsible for the tumoricidal effect. Therefore, the immunohistochemical analysis of the anti-tumor marker iNOS was also measured using tumor slices after various treatments (Figure S23). The signals of the M1 MΦ marker iNOS showed a significant increase after BK@AIE NPs plus laser treatment compared with AIE NPs plus laser or PBS plus laser. In addition, NK cells, known as “tumor killers”, also increased after the BK@AIE NPs plus laser treatment vs. PBS plus laser or AIE NPs plus laser, respectively (Figure S24).

As a result of the inspired immune system, series of representative cytokines of T cells in the serum that regulates immune responses including IL-2, IL-10, IL-12, IL-1β, IFNγ, and TNFα significantly increased after treating with BK@AIE NPs plus laser compared to AIE NPs plus laser or PBS plus laser (Figure S25). In general, IL-1β, IL-12, IFNγ, and TNFα belong to the T helper 1 (Th1) response when IL-10 belongs to the T helper 2 (Th2) response. IL-2 secretion inspires T and B lymphocyte activity, improves tumoricidal immunity, activates

microglia, and regulates Tregs. The cytotoxic immune response was promoted by IFNγ, which was mainly generated by CD4+ and CD8+ T cells, and NK cells. The microglia-secreted IL-12 could activate NK cells, and stimulate T cells during the self-stimulating circuit. While IL-10 is a multifunctional immune cytokine with antiangiogenic properties. Cytokines such as TNFα can stimulate a cell-mediated humoral immune reaction and ultimately inhibit tumor proliferation. As a local PTT, BK@AIE NPs also enhances antitumor immunity via three pathways. Firstly, PTT of AIE NPs could promote the generation of chemokines and cytokines, thereby stimulating the systemic immune response to exerting antitumor activity. The obvious increase in pro-inflammatory cytokines after PTT treatment induces acute inflammation, suggesting the occurrence of an inspired innate immune response. Secondly, PTT was identified to induce the CNS and thus activates the immune system. Thirdly, the PTT of BK@AIE NPs kills GBM cells by both necrosis and apoptosis. Then the dead tumor cells would be engulfed by innate immune effector cells, which could specifically present tumor-derived antigenic peptides to T cells to stimulate the corresponding T-cell response.

For standard treatments of chemo and radiotherapy, CSCs are inherently refractory and play a role in key aspects of disease propagation including primary tumor expansion and tumor metastasis.[58, 59] The current challenge for ablating this key subgroup can be attributed to tumor recurrence. Fortunately, heat-mediated cancer treatments represent an attractive possibility for ablating CSCs. To confirm that stem cells had a sensitivity to PTT of BK@AIE NPs, the surviving fraction was analyzed by flow cytometry. The results are shown in Figure 6G. As expected, treatment with PBS plus laser had no significant impact on all the CD133+ cell subpopulations. AIE NPs plus laser reduced the average percentage of CD133+ cell subpopulations compared to PBS plus laser. However, the BK@AIE NPs plus laser could significantly reduce the percentage of cell subpopulations. These results demonstrated that

BK@AIE NPs-mediated hyperthermia could serve as an advanced therapy for the elimination of stem cells and bulk brain cancer cells.

3. Conclusions

In summary, we have developed a multifunctional biocompatible nanoplatform based on BK coated AIE NPs, which could (i) specifically target the brain tumor, (ii) penetrate through the BTB, (iii) perform PTT, and (iv) simultaneously activate the local immune system for a very effective synergetic brain cancer therapy. *In vivo* bimodal fluorescence and MR imaging verified the significant tumor accumulation of BK@AIE NPs. *In vivo* excellent tumor inhibition effect of PTT from BK@AIE NPs was realized by systematic administration of the animal tumor models. With the advantages like the temporary modulation of BTB permeability, GBM cells could be specifically targeted, followed by a rapid increase in the local temperature of the brain tumor with minimal harm to surrounding normal tissue. *In vivo*, BK@AIE NPs-mediated PTT showed a significant effect in both eliminating tumor cells for releasing antigens in the local microenvironment and instigating an inflammatory response for recruiting immune cells into the region. BK@AIE NPs-mediated PTT is thus an apt tool for activating the immune system of the brain. Moreover, BK@AIE NPs-mediated PTT could eliminate CSCs inside tumors in mouse models, the root of cancer recurrence associated with conventional therapy, for cancer treatment with highly improved efficacy.

In future, in order to promote the clinical translation of the BK@AIE NPs, we will carefully optimize the synthesis chemistry and manufacturing process, so that the critical features of the nanomedicine such as particle size, size distribution, charges and AIE encapsulation can be well controlled. In addition, we will also carry out preclinical efficacy and safety studies in larger animals such as pigs, to better predict the response variability and therapeutic efficacy in patients.

Supporting Information ((delete if not applicable))
Supporting Information is available from the Wiley Online Library or from the author.

Acknowledgements
This work is supported by the Villum Fonden, Denmark, Project No. 13153. We are also grateful for the financial support from the Research Grant Council of Hong Kong (16305518 and C6009-17G).

Received: ((will be filled in by the editorial staff))
Revised: ((will be filled in by the editorial staff))
Published online: ((will be filled in by the editorial staff))

A multifunctional biocompatible nanoplatform based on BK@AIE NPs, which can (i) specifically target the brain tumor; (ii) penetrate through the BTB; (iii) perform PTT; and (iv) simultaneously activate the local immune system for a very effective synergetic brain cancer therapy. Moreover, BK@AIE NPs-mediated PTT can eliminate CSCs recurrence associated with conventional therapy, for cancer treatment with highly improved efficacy.

Ming Zhang, Wentao Wang*, Mohsen Mohammadniaei, Tao Zheng, Qicheng Zhang, Jon Ashley, Shunjie Liu*, Yi Sun*, Ben Zhong Tang*

Upregulating Aggregation-Induced Emission Nanoparticles with Blood-Tumor-Barrier Permeability for Precise Photothermal Eradication of Brain Tumors and Induction of Local Immune Responses